Effect of Nanochannel Geometry on DNA Structure in the Presence of Macromolecular Crowding Agent

Jeremy J. Jones,[†] Johan R. C. van der Maarel,[‡,§] and Patrick S. Doyle*[,†,‡]

[†]Department of Chemical Engineering, Massachusetts Institute of Technology, 77 Massachusetts Avenue, Cambridge, Massachusetts 02139, United States

[‡]BioSystems and Micromechanics (BioSyM) IRG, Singapore-MIT Alliance for Research and Technology (SMART) Centre, Singapore

[§]Department of Physics, National University of Singapore, Singapore

S *Supporting Information*

ABSTRACT: We experimentally and numerically study the effects of macromolecular crowding agents on DNA structure when confined to a nanochannel. Curiously, DNA response to crowding is significantly different between bulk phase, nanoslit confinement, and nanotube confinement. Coarse grained Brownian dynamics simulations reproduce trends seen in the experiments and allow us to develop a deeper understanding of the key physics at play in these systems. It is proposed that the occupancy of free volume next to the channel wall by crowders causes an effective reduction in confining dimensions of the channel that initially swells DNA in nanoconfinement.

KEYWORDS: DNA, confinement, crowding, nanochannel, nanofluidic, biophysics
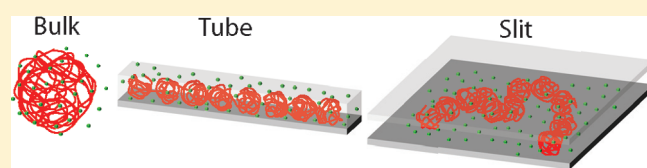
Most biological media are physically crowded systems that contain a large volume fraction of macromolecules.[1] A large number of the molecules have no specific affinity for one another, however these essentially inert crowding agents can have a profound impact on thermodynamic activities of reactants and molecular structure.[2,3] Biologically inspired studies that explore alterations to molecular structure have mostly focused on the role of low concentrations of Mg^{2+} ions and other multivalent cations in compaction of polyelectrolytes.[4−6] As such, the effect of charge neutral crowding agents on molecular structure and function has in large remained under appreciated. Recently, condensation of DNA using neutral osmotic agents has gained attention because of its realized importance in a variety of biological processes such as understanding the structure of the nucleoid in bacteria[7,8] and ejection of DNA from phages,[9,10] and its possible application in gene therapy.[11,12] Classic polymer-salt induced condensation, or ψ-condensation, of DNA has been a well-studied problem since Lerman's original work.[13,14] This phenomenon results from overthreshold concentrations of neutral polymers forcing a depletion-induced first order phase transition. It has been common for these in vitro studies to ignore other biologically relevant immobile structures, such as lipid membranes and cytoskeletal filaments, which act to produce steric constraints and a confinement environment.

Nanofabrication offers an attractive route to develop model confined geometries. Among the myriad of possible geometries, slits, and tubes serve as canonical examples of uniaxial and biaxial confinement respectively. Static and dynamic properties of DNA in nanoslits have been measured as a function of channel height,[15−17] molecular weight,[18,19] and buffer ionic strength.[20]

Likewise, DNA extension in nanotubes has been measured as a function of channel width[21,22] and ionic strength.[23−25] Recently Zhang et al.[26] studied how addition of a neutral macromolecular crowding agent, dextran, to DNA confined in a nanotube affects the equilibrium coil size. Converse to bulk osmotic agent studies, they observed that the nanotube confined DNA initially swells with addition of dextran and then abruptly condenses into a globular form. They also found that the first order transition to globular form occurs at significantly lower volume fractions than seen in bulk. Their results demonstrate that confinement plays a significant role in DNA response to depletion agents. It is natural to wonder whether other forms of confinement will have similar effect or if the nanotube geometry is somehow unique.

Here, we experimentally study the effects of crowding agents on both the structure and dynamics of single DNA molecules in bulk and confined to nanoslits. Inspired by Zhang et al.,[26] we use dextran and focus on a crowder concentration range that is well below that required for DNA compaction in bulk (unconfined).[27] The DNA coil size in nanoslits is seen to nonmonotonically change with dextran concentration. Given previous observations in nanotubes, it was anticipated that the nanoslit confinement would differ from the bulk phase behavior. However, significant differences between the two types of channels (slits versus tubes) show that confinement geometry plays an important role. We develop a simple Brownian dynamics algorithm that contains the essential physics necessary to qualitatively and semiquantitatively
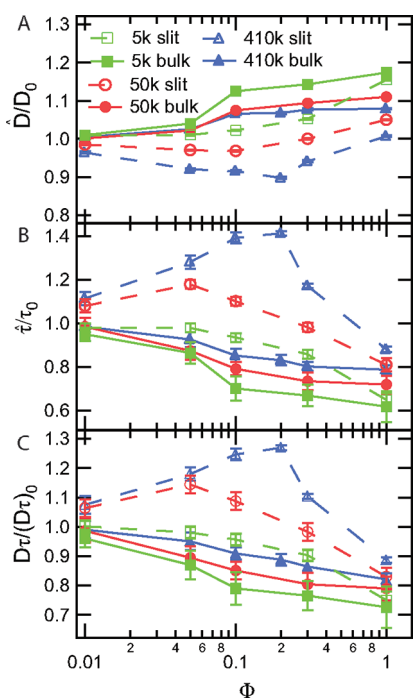
Figure 1. Normalized experimental measurements of the (A) diffusion coefficient, (B) longest relaxation time, and (C) effective mean squared coil size of λ-DNA in bulk and nanoslit confinement as a function of dextran concentration for three different dextran sizes: 5, 50, and 410k. Solid lines and symbols indicate bulk experiments, and the dashed lines with open symbols correspond to slit channel experiments (H = 250 nm). D_0 and τ_0 indicate the diffusion coefficient and rotational relaxation time for λ-DNA with $\Phi = 0$.

reproduce the trends seen in both nanoslits and nanotubes. The simulations allow us to explicitly track the nanoscale depletants that give insight into the mechanism responsible for the unusual DNA behavior.

Single Molecule Experiments. Equilibrium dynamic and static properties of λ-DNA (48.5 kbp, New England Biolabs) were measured in glass nanoslits using the image acquisition and analysis method outlined in a previous article.[18] Straight glass nanoslit channels of height H = 250 nm, were fabricated by a photoresist protected etch in buffered oxide etchant and thermally bonded to a glass cover slide as described by Mao et al.[28] λ-DNA were stained with YOYO-1 dye (Invitrogen) at 4 base pair per dye molecule and diluted in 1 × TE (10 mM Tris base and 1 mM EDTA),(Omnipure) that contained 4 % vol β-mercaptoethanol (Cabiochem). The DNA was incubated in the staining solution for at least 12 h. The stained DNA solution was then diluted (5−7)-fold into a mixture containing the desired concentration of dextran. This final buffer was incubated for at least 24 h before the microscopy experiments. The solution ionic strength was estimated to be 13.4 mM and viscosity was found to be 1.09 cP. Dextran was used as our model crowder. It is a neutral branched polysaccharide made of glucose monomers and is frequently used to mimic a crowded medium in vitro because of its inert behavior.[2] Dextran readily dissolves in most solutions and essentially acts as a nanosphere suspension. The dextran used in this study have molecular weights of 5, 50, and 410 kg/mol (Sigma Aldrich - Fluka, analytical standard, GPC) with radius of gyration (R_g) of 2.6, 6.9, and 17.1 nm, respectively, ($R_g = 0.066 \times MW^{0.43}$ with MW in g/mol and R_g in nm[29]).

A uniform electric field (typically 20−50 V/cm) was produced across the channel using an external DC power source and was used to drive DNA into the channel. Once the DNA was brought into the observation field of view the electric field was shut off and the molecules were allowed to relax to equilibrium for at least 60 s before image acquisition. Each experimental data point in Figure 1 is composed of an ensemble average of 35−50 different molecules. Molecules were imaged for approximately 2 min at 30 frames/s.

The diffusion coefficient and rotational relaxation time were measured at different concentrations of dextran (Figure 1). To remove viscosity effects from the data we define a scaled diffusivity $\hat{D} = (D\eta/\eta_o)$ and scaled relaxation time $\hat{\tau} = (\tau\eta_o/\eta)$ where the reference viscosity, η_o, is taken as the buffer viscosity. At our probing frequency and dextran concentrations, we find that the solution rheology is described by a Newtonian fluid and use particle tracking microrheology to determine the viscosity (Supporting Information). We normalize the dynamic measurements by the pure buffer values of $D_0 = 0.41 \pm 0.01$ μm^2/s and $\tau_0 = 0.10 \pm 0.01$ s in the bulk, and $D_0 = 0.11 \pm 0.01$ μm^2/s and $\tau_0 = 0.79 \pm 0.01$ s in the 250 nm nanoslit. Following Zhang et al.,[26] we choose to write concentration in terms of an effective volume fraction in which it is assumed that the dextran occupy a hard sphere volume defined by their radius of gyration, R_g. Therefore $\Phi = (4NR_g^3\pi)/(3V)$ where N is the number of dextran in solution and V is the volume of the solution. This definition for concentration affords a more intuitive understanding of the volume occupied by the crowders. A volume fraction of unity corresponds to the overlap concentration and thus all our dextran solutions are in the dilute regime. In Figure 1C an effective coil size is inferred by recognizing that the product of $D\tau \propto R_\parallel^2$.[18,30] We choose to use this measurement of coil size because diffusivity and rotational relaxation time can be more accurately determined than coil size from microscopy experiments.[17]

For unconfined DNA (bulk), we find that the DNA size monotonically decreases with increasing dextran concentration (Figure 1C) and that dynamic properties vary with respect to DNA size as we would expect. Hence, the diffusion coefficient increases with reduction of coil size (Figure 1A) while the relaxation time decreases (Figure 1B). We explain the monotonic bulk coil size change by an inward osmotic pressure induced by a slight depletion of the dextran from the interior of the DNA coil. Following a procedure originally proposed by de Gennes[31,32] and later reproduced by Zhang et al.,[26] we express the density difference between the interior and the exterior a the DNA coil as $\Delta\rho \approx \Phi(4/3\pi)^{-1}R_g^{-5/3}R_{coil}^{-4/3}$, where R_{coil} is the DNA coil size and R_g is the dextran radius. The osmotic pressure due to the crowders is simply $\prod_{osmo} = kT\Delta\rho$. Thus, with increasing dextran concentration there is an increase in the isotropic inward osmotic pressure resulting in a reduction of coil size. At a given volume fraction, the osmotic pressure is greater for smaller dextran, therefore a more significant coil size reduction is observed in the bulk phase. Notice, we do not see the depletion induced first order transition into the globular form for our range of volume fractions. We found that a volume fraction of $\Phi \sim (3-4)$ for the smallest dextran (5 kg/mol) are required to induced condensation of unconfined (bulk) DNA. Our results are unique in that we study DNA structure at significantly lower concentrations of crowders than other condensation studies. Though these results are not surprising, we do find it intriguing that we are able to resolve the subtle size reduction. Other researchers have reported experimental results in polyethylene glycol that display slight

reductions in coil size before the first order transition.[14,27] However, these trends were discounted because the size reduction was on the order of the data error. Such reduction in DNA coil size is analogous to adjusting ionic strength or temperature. By incorporating crowders, we are effectively modulating the solvent quality. This is also the first time to our knowledge that both DNA diffusion coefficient and rotational relaxation time have been systematically studied for large molecular weight dsDNA in the presence of crowding agents. There have been studies on diffusion of short dsDNA in crowding agents in the context to understand rheology of the dextran solution.[33,34]

The more striking observation in our experiments is that in nanoslits we observe a nonmonotic change in DNA size with increasing concentration of dextran. As seen in Figure 1C, the DNA coil initially swells, reaches an apex, and eventually compresses with further increase in dextran volume fraction. This swelling behavior is contrary to the observed isotropic compression of DNA in bulk phase. It is expected that the DNA unconfined dimensions are still exposed to the osmotic compressive force from the dextran thereby causing a reduction in the in-plane coil size. Hence, the increase in DNA coil size suggests that there is an swelling force that initially dominates and counteracts the inward, in-plane osmotic pressure. We further addressed the cause of swelling later in this letter. For large molecular weight dextran the coil size at the apex is larger and is shifted to higher volume fractions. Akin to the bulk experiments, we always observe a larger DNA coil size for the larger dextran at a given Φ. A first order phase transition into globular state is not observed in nanoslits for the volume fractions studied. The decent from coil size apex is much steeper than the isotropic size decrease seen in bulk.

Having experimentally explored nanoslit confinement, it now behooves us to review results in nanotube confinement with dextran. Zhang et al.[26] performed single molecule experiments on T4 DNA in 300 nm wide nanotubes and used the same dextran crowders. They found equally surprising results when comparing to bulk studies. In their experiments, the DNA response to dextran can be separated into two regimes: a subthreshold dextran concentration regime characterized by DNA elongation along nanotube and an overthreshold dextran concentration regime in which the DNA condenses into a compact structure. These results are unique from the unconfined case in two aspects. First, the subthreshold volume fractions of dextran result in elongation of DNA similar to nanoslits. In bulk phase, swelling is never observed. Second, the DNA condenses into globular form at significantly lower volume fraction than found in bulk. This compaction occurs as a first order transition and differs from the gradual contraction in coil size in nanoslits.

There are remarkable parallels between the nanoslit and nanotube confinement. We first consider similarities between confinement geometries in the low dextran volume fraction regime. In both channel types, we see an expansion of the DNA coil. When set against volume fraction, the growth induced by different dextran sizes collapse to a single master curve for nanotubes. This also seems to be the case for nanoslits, though the collapse is not as uniform. The swelling is not observed in bulk phase therefore we deduce such behavior is prompted by nanoconfinement. Additionally, we find similar trends at the transition points for the two geometries. The critical dextran volume fraction for DNA condensation in nanotubes is proportional to the dextran size. This observation is rationalized by an attractive depletion interaction between DNA segments due to

exclusion of nanoparticles from the overlap of the cylindrical depletion volumes around DNA segments.[26] Observations in nanoslits are similar in that, the apex of coil size swelling occurs at a volume fraction nearly proportional to dextran size. However, the reason for this is not as clear as nanotubes.

Our results show very plainly that confinement geometry plays a role in DNA response to crowding. Most notably, the DNA undergoes an abrupt transition from a coil to a compact globular form in nanotubes while there is no such collapse in nanoslits. Reduction in DNA coil size in nanoslits occurs over a large range of crowder concentrations and does not compact to the same extent as tubes. Also, though both geometries show an initial increase in coil size, in nanotubes the DNA swells a greater extent than nanoslits. At maximum extension, DNA in-plane radius swells ~40% in tubes and only ~14% in slits.

Brownian Dynamic Simulations. The experimental results leave several compelling questions. What gives rise to the swelling seen in confinement? Why do slits and tubes differ? To better understand these systems we performed Brownian dynamic simulations. First, we must expound the important physics involved. We can identify four essential attributes in our system. (1) Dextran interacts with its surroundings as a volume filling body absent other specific interactions. (2) The DNA must have connectivity between adjacent segments to account for entropic elasticity. (3) We must consider excluded volume between DNA segments. (4) Finally, we must account for the confinement imposed by the nanochannel.

We choose to develop a coarse grained model which contains these essential physics. Our model crowder, dextran, mainly interacts via steric repulsions and its highly branched structure gives the particles a nearly spherical shape. Therefore, we model our dextran—DNA interactions with hard spheres. To reduce computational cost we do not incorporate dextran—dextran interactions. One can justify this approach by recognizing that the dextran suspension is in the dilute regime. We use a soft repulsion potential developed by Jendrejack et al.[35] to incorporate excluded volume between DNA beads and adjacent beads are connected by a modified wormlike chain.[36] Our method for simulating DNA in confinement is similar to Tang et al.[17] in which wall—DNA, wall—dextran, and DNA—dextran interactions are resolved using a hard sphere Heyes—Melrose algorithm.[37,38] Details of our Brownian dynamics simulation can be found in the Supporting Information. The model is admittedly simplified and does not account for subpersistence length phenomena such as bending energies. These effects are of course important but, as we will show, not essential to reproduce the trends seen in all of the experiments. Hence, we feel simplicity in our model affords more clarity in elucidating the mechanism at play.

We find that the Brownian dynamics simulations qualitatively and semiquantitatively capture the trends seen in experiments. Figure 2A shows simulation results of the mean squared in-plane radius of gyration, $\langle R_{\parallel}^2 \rangle$, of λ-DNA in bulk and slit nanochannel. We compare these results to the effective mean squared coil size from experiments, Figure 2B. In the bulk phase simulation we see the characteristic monotonic coil size reduction with addition of dextran. Again, the smaller dextran induces a more profound size change. The extent of coil size change is not as significant in the simulations compared to experiments, though of comparable magnitude. Simulations of DNA in confinement however show significant nonmonotonic behavior with addition of the largest dextran (410k), a trend that is much less profound with the
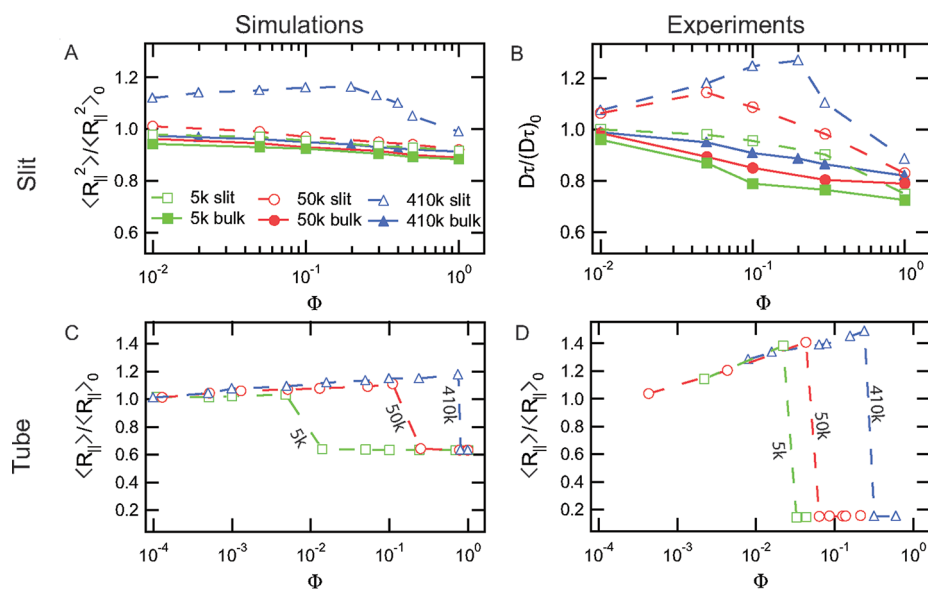
Figure 2. Upper graphs show (A) in plane squared radius of gyration from Brownian dynamic simulations and (B) experimental measurements of effective mean squared coil size for λ-DNA in bulk and slit channel confinement. Lower plots include (C) normalize mean extension for simulations of λ-DNA in tube (width 250 nm) compared to (D) Zhang et al.[26] experimental measurements of T4-DNA mean extension (tube width 300 nm). Solid lines and symbols indicate bulk and the dotted lines with open symbols correspond to channels. $\langle\rangle$ represents an ensemble average quantity.

smaller dextran. The degree of swelling for the largest dextran is on the same order of magnitude as our experimental results and the swelling apex is found at a similar volume fraction. Impressively, the simulations were able to reproduce not only the second order trend seen in the nanoslit experiments, but we are also able to reproduce the trends with dextran size. We demonstrate how this swelling becomes more pronounced with larger dextran beads in the Supporting Information.

Since we are able to successfully replicate experimental observations in nanoslits using our simulation algorithm, we now turn our attention to nanotubes. It is desirable to compare nanoslit results with an analogous model for tubes. Hence, we simulate λ-DNA in a square cross section conduit with tube side length, H = 250 nm (Figure 2C). These results are compared with the Zhang et al.[26] experimental results for T4 DNA in 300 nm wide nanotubes (Figure 2D). Unlike the nanoslits, we characterize the DNA size by the mean axial extension of the DNA, $\langle R_{\parallel} \rangle$ which was the measurable in the experiments of Zhang et al. Both simulations and experiments in nanotubes show an initial swelling of the DNA coil with increasing dextran concentration followed by an abrupt transition into a globular state. We see that the transition point occurs at similar volume fractions for the simulations and experiments. The simulations also capture the collapse of $\langle R_{\parallel} \rangle$ for different dextran onto a master curve when plotted against volume fraction. The ability to capture the trends in both channel geometries without adjusting parameters is a testament to the essential physics we postulated were necessary to include in the model. Not surprisingly, there are however some differences between nanotube simulations and experiments. Simulations show less elongation than experiments, and the globular form does not compress to the same degree. We attribute these to the simplicity of the coarse grained system. For example, by modeling DNA sections by hard spheres we inherently limit the extent of compaction allowed.

Swelling is only observed in confinement and as such we attribute this effect to the coupling of confinement and crowding.

Zhang et al.[26] originally proposed that the channel wall could lend to an anisotropic osmotic pressure that explains this behavior. It is well-known that the polymer segment density is smaller near a surface because there is a configurational entropic penalty for bringing the center of mass near a surface. In experiments, we expect the DNA to be depleted near the wall in a region on the order of its persistence length, $l_{\mathrm{p}} \approx 50$ nm, which is larger than our largest dextran. Therefore, the dextran is able to access this DNA depleted region near the channel wall resulting in a noncompensating pressure transverse to the wall. This osmotic pressure drives DNA segments away from the channel wall and further concentrates it near the channel center. However, this increased segment density results in an unfavorable increase in the free energy due to intramolecular excluded volume interactions and so the chain will instead swell in the directions parallel to the channel surfaces as a result. We show in Figure 3 the simulation DNA probability distributions, P, and normalized dextran density distributions, ρ/ρ_0, transverse to the slit wall. Without dextran in the system, the DNA tends to be slightly depleted from the channel wall resulting in a larger DNA density near the channel center. When dextran concentration is increased the DNA beads tend to focus more toward the center of the channel and repulsive excluded volume interactions between chain segments cause in-plane swelling of the coil. When comparing Figure 3 panels A and C we see that the larger dextran induces a more profound compression transverse to the channel wall. It is clear from Figure 3B that there is a depletion of the largest dextran from the center of the DNA coil relative to the channel wall. The gradient in dextran density results in an osmotic pressure which must be compensated by extension in the planar direction. The smaller dextran (Figure 3D) can more easily occupy the interior of the DNA coil and results in a less significant extension.

The arguments above suggest that the observed in-plane swelling should be directly correlated to a decrease in the transverse DNA size $R_{\perp}$. To explore this idea in more detail, we first recall
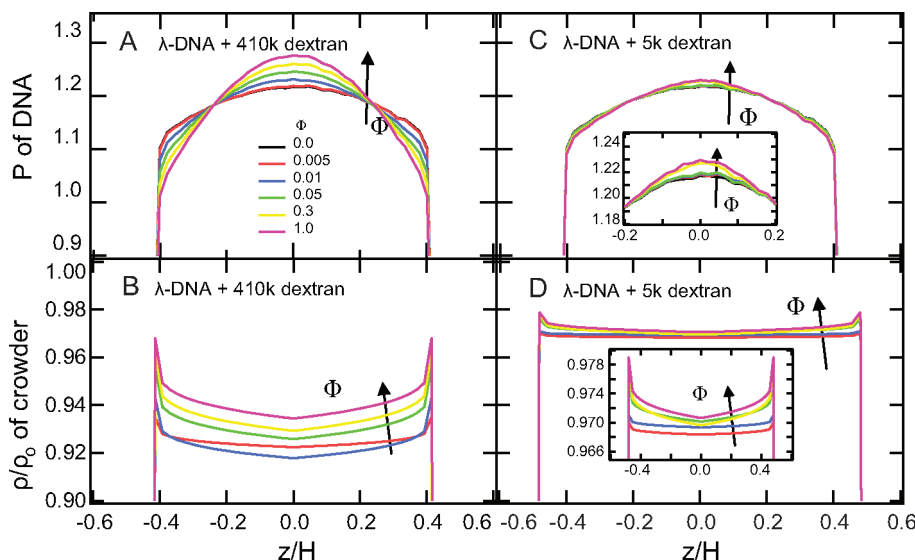
Figure 3. Simulation results for DNA probability profiles and normalize dextran density profiles in transverse direction of nanoslit for (A,B) 410k dextran and (C,D) 5k dextran from simulations. The inlays in C and D show an enhanced magnification at the cusp of the density profiles. Arrows indicate the direction of increasing dextran concentration.
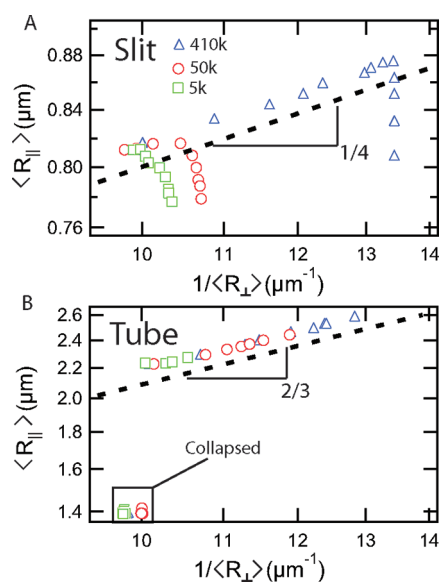
Figure 4. Simulations of in-plane mean size of DNA versus the inverse perpendicular mean size in (A) slit and (B) tube confinement. This perpendicular mean size is a measure of the blob size in confinement. The dotted lines are the scalings given by eq 2.

classic results from blob scaling arguments in the absence of crowding agents. In our confining systems, we can imagine the DNA as being comprised of individual blobs[39,40] with uniform size. In a slit, these blobs follow a two-dimensional self-avoiding walk and in a tube the blobs are linearly packed

$$R_\parallel^{tube} \sim R_b N_b, \qquad R_\parallel^{slit} \sim R_b N_b^{3/4} \qquad (1)$$

where R_b is the blob size, N_b is the number of blobs, $R_\parallel^{tube}$ is the mean extension for the DNA inside a tube, and $R_\parallel^{slit}$ is the mean radial size of the in-plane coil in a slit. We can further write $N_b = N/g$ where N is the number of statistical segments in the DNA chain and g is the number of statistical segments in a single blob.

To maintain the bulk statistics of the blobs the number of segments per blob of size R_b is $g \sim (R_b/b)^{5/3}$. Here we represent a chain statistical segment length as b. Hence, the in-plane size of the DNA in slits and tubes scales with blob size as

$$R_\parallel^{tube} \sim R_b^{-2/3}, \qquad R_\parallel^{slit} \sim R_b^{-1/4} \qquad (2)$$

In the absence of crowding agents, the blob size is assumed to be the length of channel's confining dimension (e.g., slit height) and from equation eq 2 we recover the predicted relation between in-plane swelling and channel size. In the current studies we fix channel height but argue that R_b changes due to the compressive forces of crowding agents. We further assume that $R_b \sim R_\perp$ to obtain the following predicted correlations

$$R_\parallel^{tube} \sim R_\perp^{-2/3}, \qquad R_\parallel^{slit} \sim R_\perp^{-1/4} \qquad (3)$$

We compare these scalings with our simulation results in Figure 4 where we present a log−log plot of $R_\parallel$ versus $R_\perp$. During the DNA swelling phase in slits (Figure 4A) we see that the extension follows the blob scaling. After reaching the extension apex the simulation results deviate from the scaling. This deviation point corresponds to where the in-plane osmotic stress starts to be appreciable and this is not accounted for in the scaling argument. DNA extension in tubes (Figure 4B) is also well described by the scaling throughout the DNA elongation phase. Importantly, data in the swelling phase for both slits and tubes collapse onto a master curve. The close agreement with the scalings in eq 3 and master curve collapse lend strong support to our hypothesis that chain swelling is driven by the crowder-induced compression of the chain in the transverse direction. We can also define an effective reduced channel height due to the crowders using the relation $H_{eff} = H \times (\langle R_\perp \rangle / \langle R_\perp \rangle_{\phi=0})$. Using this relation we find that the maximum effective channel height reduction in a tube is $\sim$40 nm and in a slit is $\sim$43 nm. These occur for the 410k dextran which we recall has a diameter of 34 nm; comparable to the channel height reduction. The concept of effectively reducing channel height via excluded volume interactions is also seen in
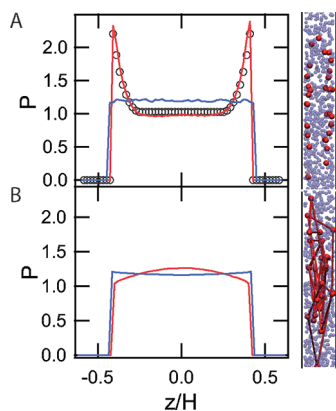
Figure 5. Probability distribution for the simulated DNA beads (solid red line) and dextran beads (solid blue line). (A) Simulation of DNA beads once springs between beads are removed and allowed to freely diffuse compared with (B) connectivity still in place. Black circle markers indicate theory results based on standard Asakura−Oosawa theory.[45] Simulation snapshots of DNA (red beads) and dextran (blue beads). To improve clarity every second dextran bead is shown in the snapshot. Simulation conditions: R_g = 17.1 nm (410k), Φ = 0.3 and H = 250 nm.

the overlapping regions of highly confined DNA during hairpin formation.[41]

We must now address why slits and tubes differ. In the low volume fraction regime, the extension along the channel walls is explained by the dextran occupancy of free volume along the channel wall mechanism. However, in the nanotubes the DNA in confined in two dimensions. This means that there is a polymer depletion layer near four walls which results more free volume for the dextran to occupy as compared to the nanoslit. Thus, the compression force transverse to the channel wall is more significant for the nanotube and results in a larger extension. Or, more simply displayed, the extension dependence on blob size is more strongly associated in tubes than slits. The unconfined dimensions of DNA are subjected to a compressive inward osmotic pressure that acts to shrink coil size. In slits, the blobs composing the DNA coil are able to rearrage themselves because they have two degrees of freedom to do so. However, while in nanochannels, these blobs lack the ability to rearrange into a more favorable manner therefore they must elongate or condense. We never observe this collapse in slits or bulk, however we do expect the DNA to eventually collapse at larger dextran concentrations and/or ionic strengths.

When interpreting results we should consider several important differences between our simulations and experiments and the experiments of Zhang et al.[26] There are three significant differences between our simulations/experiments and Zhang et al. experiments. First, we use λ-DNA as our model polymer. Changes in polymer size alter the balance of entropic to excluded volume energies. Second, our channel height is about 50 nm smaller. Again, altering the degree of confinement plays a part in changing the free energy of the system. Lastly, the ionic strength in this Letter (∼13 mM) is larger than that used in the nanotube experiments by Zhang et al. (∼3 mM). The smaller ionic strength will result in a more significant excluded volume effect and an increase in DNA effective width[42,43] and persistence length.[44] Fortunately, Zhang et al. did find that results were qualitatively similar for ionic strengths spanning at least an order of magnitude (they tested ionic strengths ranging from ∼3−30 mM).

The diminished DNA segment density near a hard surface is related to the connectivity of the chain and the entropic penalty of compressing a polymer as it approaches a surface. To better demonstrate the importance of DNA connectivity in the elongation mechanism, we remove the springs in our Brownian dynamic simulation. Figure 5 compares probability densities of DNA and dextran beads in the transverse direction to a nanoslit wall. The DNA beads tend to be located near the walls when connectivity is removed. This localization near the boundaries can be realized by considering short-range depletion interactions in a colloidal dispersion. In our simulations, the DNA beads are larger than the dextran beads. When the DNA beads approach within a dextran diameter of the channel wall there will be an attractive interaction between the wall and the bead. This occurs because the smaller dextran beads are depleted from the volume between the larger particle and the wall thereby creating a noncompensating pressure toward the wall. We can predict the probability profiles for this system using assumptions presented by Asakura−Oosawa (see Supporting Information).

Conclusions. Our observations demonstrate that DNA behavior in the presence of crowding agents is highly dependent on the confinement geometry. In particular, swelling of DNA coil occurs due to occupancy of free volume along the channel walls by dextran crowders. Macromolecular crowders such as dextran are typically used to mimic the cellular environment. These results show the necessity of accounting for confinement in understanding the effect of crowding on biophysical systems. There is interest in understanding crowding's contribution to actin filament bundling and the shape of the nucleoid. *In vivo*, biological surfaces such as bilipid membranes and other surrounding cytoskeletal filaments create a naturally confined environment and therefore cannot be neglected. Furthermore, with increasing importance of nanofluidic devices in single molecule DNA research it is necessary to effectively manipulate DNA. By tuning crowding concentration, one may alter DNA configuration by adjusting the solvent quality of the surrounding medium and by effectively shrinking the confining dimension. Though our model provides convincing support for this mechanism, it is recognized that these simulations are relatively simple and other effects could help contribute to the nonmonotonic behavior seen. For instance, it is known that under some conditions that correlations between crowders can dramatically alter the phase diagram.[46,47] More thorough simulations should be done in the future to determine if and how interactions between dextran particles would change our results. Also, there are potentially electrostatic interactions between the DNA and the channel wall. Hence, in the case where the Debye layer is on the same order of the channel height there will be a reduction in the effective dimension due to co-ion depletion near the channel wall. This could lead to freeing of more volume near the wall and could result in a more profound swelling effect.

■ ASSOCIATED CONTENT

Ⓢ Supporting Information. Description of how dynamic and static measurements are made from fluorescent microscopy movies; DNA anisotropy measurements; description of Brownian dynamic simulations; description of microrheology results for dextran solution; additional density profiles for simulations of slit and tube channels; blob size to channel height factor; simulations of DNA in slits with larger dextran; and theory for Asakura-Oosawa depletion interaction with channel wall. This

material is available free of charge via the Internet at http://pubs.acs.org.

■ AUTHOR INFORMATION

Corresponding Author
*E-mail: pdoyle@mit.edu.

■ ACKNOWLEDGMENT

■ REFERENCES

(1) Minton, A. P. *J. Cell Sci.* **2006**, *119*, 2863–2869.

(2) Zimmerman, S. B.; Minton, A. P. *Annu. Rev. Biophys. Biomol. Struct.* **1993**, *22*, 27–65.

(3) Zhou, H. X.; Rivas, G.; Minton, A. P. *Annu. Rev. Biophys.* **2008**, *37*, 375–397.

(4) Thoma, F.; Kuller, T.; Klug, A. *J. Cell Biol.* **1979**, *83*, 403–427.

(5) Giannasca, P. J.; Horowitz, R. A.; Woodcock, C. L. *J. Cell Sci.* **1993**, *105*, 551–675.

(6) Hansen, J. C. *Annu. Rev. Biophys. Biomol. Struct.* **2002**, *31*, 361–392.

(7) Odijk, T. *Biophys. Chem.* **1998**, *73*, 23–29.

(8) Cunha, S.; Woldringh, C. L.; Odijk, T. *J. Struct. Biol.* **2001**, *136*, 53–66.

(9) Evilevitch, A.; Lavelle, L.; Knobler, C. M.; Rapaud, E.; Gelbart, W. M. *Proc. Natl. Acad. Sci. U.S.A.* **2003**, *100*, 9292–9295.

(10) Jeembaeva, M.; Castelnovo, M.; Evilevitch, A. *J. Mol. Biol.* **2008**, *381*, 310–323.

(11) Millili, P. G.; Selekman, J. A.; Blocker, K. M.; Johnson, D. A.; Naik, U. P.; Sullivan, M. O. *Microsc. Res. Tech.* **2010**, *73*, 866–877.

(12) Vijayanathan, V.; Thomas, T.; Thomas, T. *J. Biochem.* **2002**, *41*, 14085–14094.

(13) Lerman, L. S. *Proc. Natl. Acad. Sci. U.S.A.* **1971**, *68*, 1886–1890.

(14) Vasilevskaya, V. V.; Khokhlov, A. R.; Matsuzawa, Y.; Yoshikawa, K. *J. Chem. Phys.* **1995**, *102*, 6595-6602. 18.

(15) Bonthuis, J. D.; Christine, M.; Stein, D.; Dekker, C. *Phys. Rev. Lett.* **2008**, *101*, 108303.

(16) Uemura, H.; Ichikawa, M.; Kimura, Y. *Phys. Rev. E* **2010**, *81*, 051801.

(17) Tang, J.; Levy, S.; Trahan, D.; Jones, J. J.; Craighead, H.; Doyle, P. S. *Macromolecules* **2010**, *43*, 7368–7377.

(18) Hsieh, C.-C.; Balducci, A.; Doyle, P. S. *Macromolecules* **2007**, *40*, 5196–5205.

(19) Lin, P.-K.; Fu, C.-C.; Chen, Y.-L.; Chen, T.-R.; Wei, P.-K.; Kuan, C. H.; Fann, W. S. *Phys. Rev. E* **2007**, *76*, 011806.

(20) Hsieh, C.-C.; Balducci, A.; Doyle, P. S. *Nano Lett.* **2008**, *3*, 2–7.

(21) Reisner, W.; Mortan, K. J.; Riehn, R.; Wang, Y. M.; Yu, Z. N.; Rosen, M.; Sturm, J. C.; Chou, S. Y.; Frey, E.; Austin, R. H. *Phys. Rev. Lett.* **2005**, *94*, 196101.

(22) Persson, F.; Utko, P.; Reisner, W.; Larsen, N. B.; Kristensen, A. *Nano Lett.* **2009**, *9*, 1382–1385.

(23) Reisner, W.; Beech, J. P.; Larsen, N. B.; Flyvbjerg, H.; Kristensen, A.; Tegenfeldt, J. O. *Phys. Rev. Lett.* **2007**, *99*, 3–6.

(24) Zhang, C.; Zhang, F.; van Kan, J. A.; van der Maarel, J. R. C. *J. Chem. Phys.* **2008**, *128*, 225109.

(25) Kim, Y.; Kim, K. S.; Kounovsky, K. L.; Rakwoo, C.; Jung, G. Y.; dePablo, J. J.; Jo, K.; Schwartz, D. C. *Lab Chip* **2011**, *11*, 1721–1729.

(26) Zhang, C.; Shao, P. G.; van Kan, J. A.; van der Maarel, J. R. C. *Proc. Natl. Acad. Sci. U.S.A.* **2009**, *106*, 16651–16656.

(27) Kojima, M.; Kubo, K.; Yoshikawa, K. *J. Chem. Phys.* **2006**, *124*, 1–4.

(28) Mao, P.; Han, J. *Lab Chip* **2005**, *5*, 837–844.

(29) Senti, F. *J. Polym. Sci.* **1955**, *17*, 527–546.

(30) Rubinstein, M.; Colby, R. H. *Polymer Physics*; Oxford University Press: New York, 2003.

(31) de Gennes, P.-G. C. R. *Acad. Sci. Paris* **1979**, *288*, 359–361.

(32) Odijk, T. *Macromolecules* **1996**, *29*, 1842–1843.

(33) Dauty, E.; Verkman, A. S. *J. Mol. Recognit.* **2004**, *17*, 441–447.

(34) Dix, J. A.; Verkman, A. S. *Annu. Rev. Biophys.* **2008**, *37*, 247–265.

(35) Jenderjack, R. M.; Graham, M. D. *J. Chem. Phys.* **2002**, *116*, 7752–7759.

(36) Underhill, P. T.; Doyle, P. S. *J. Rheol.* **2006**, *50*, 513–529.

(37) Kim, J. M.; Doyle, P. S. *J. Chem. Phys.* **2006**, *125*, 074906.

(38) Heyes, D. M.; Melrose, J. R. *J. Non-Newtonian Fluid Mech.* **1993**, *46*, 1–28.

(39) Brochard, F.; de Gennes, P. *J. Chem. Phys.* **1977**, *67*, 52–56.

(40) Daoud, M.; de Gennes, P. *J. Phys. (Paris)* **1977**, *38*, 85–93.

(41) Levy, S. L.; Mannion, J. T.; Cheng, J.; Reccius, C. H.; Craighead, H. G. *Nano Lett.* **2008**, *11*, 3839–3844.

(42) Stigter, D. *J. Colloid Interface Sci.* **1975**, *53*, 296–306.

(43) Stigter, D. *Biopolymers* **1977**, *16*, 1435–1448.

(44) Dobrynin, A. V. *Macromolecules* **2006**, *39*, 9519–9527.

(45) Asakura, S.; Oosawa, F. *J. Polym. Sci.* **1958**, *33*, 183–192.

(46) Castelnovo, M.; Gelbart, W. M. *Macromolecules* **2004**, *37*, 3510–3517.

(47) de Vries, R. *J. Chem. Phys.* **2006**, *125*, 014905.